iJRASET
International Journal For Research in Applied Science and Engineering Technology

INTERNATIONAL JOURNAL FOR RESEARCH

IN APPLIED SCIENCE & ENGINEERING TECHNOLOGY

Volume: 13 **Issue:** II **Month of publication:** February 2025

DOI: https://doi.org/10.22214/ijraset.2025.67107

www.ijraset.com

Call: 08813907089 | E-mail ID: ijraset@gmail.com

International Journal for Research in Applied Science & Engineering Technology (IJRASET)
ISSN: 2321-9653; IC Value: 45.98; SJ Impact Factor: 7.538
Volume 13 Issue II Feb 2025- Available at www.ijraset.com

Removal of Phenol Using Rice Husk Doped Iron Oxide Nanoparticles with Performance, Characterization, Kinetic & Isotherm Study from Waste Water

Mahesh Patel[1], Dharmendra Patel[1], Parwathi Pillai[2*]
[1]*Department of Chemistry, Swarrnim Institute of Science, Swarrnim start-up & Innovation University, Gandhinagar 382420, India*
[2]*Department of Chemical Engineering, Swarrnim Institute of Technology, Swarrnim start-up & Innovation University, Gandhinagar 382420, India*

Abstract: ***The effluent containing phenol is one of the major health concerns for humans and the environment. Iron oxide nanoparticle (Fe NPs) has properties like size, large surface area, and magnetic nature that were more impressive for removing phenol from the aqueous solution. Batch adsorption tests for the removal of phenol from synthetic phenol water were done in the current work, and the modified iron oxide nanoparticle with rice husk ash (RH+Fe) was confirmed by characterization techniques like XRD, FTIR, SEM, and particle size analysis. Using 2.6 g/L, 50 ℃, and 10 ppm of adsorbent dosage, starting concentration, and temperature of RH+Fe, 96 % of the Phenol was removed. The RH+Fe adsorbent data were best fitted for Langmuir isotherm and had an adsorption capacity of 90 mg g^{-1}. In the kinetic investigation, the regression coefficient of pseudo-second order was determined to be 0.96. The results of the current investigation offer a promising phenol elimination adsorbent.***

Keywords: Phenol, Silica Nano, Rice husk, Iron oxide, Adsorption

I. INTRODUCTION

Globally, organic pollutants, in particular, pose a severe threat to both human health and the health of natural ecosystems. Certain organic pollutants represent a significant risk to both human health and the health of natural ecosystems on a global scale. Phenol is a hazardous pollutant for human health because of its powerful capacity to permeate the skin and mucosal barriers and its effects on the nervous and cardiovascular systems (Dong et al., 2020). According to several studies, concentrated phenol can result in severe skin lesions. Deaths caused by poisoning do occur. In fact, phenol consumption (5-500 mg) whether accidental or intentional, is regularly associated with baby fatalities. But, if an adult consumes 1-32 g, adult mortality may result (Ge et al., 2018). The presence of phenol in wastewater is a significant problem since it is hazardous to aquatic life and, at concentrations on the order of ppb (parts per billion), it gives water a particularly foul odour and flavour. Hence, removing phenol in an economical and environmentally responsible method is a good strategy to safeguard human health as well as the environment (Ahmadi and Igwegbe, 2018).

To date, numerous techniques have been suggested to eliminate phenols from wastewater. For instance, some of the most widely utilised techniques include chemical precipitation, electrochemical oxidation, photochemical processes, ozonation, ion exchange, and chemical and Fenton processes (Mandal et al., 2019). Adsorption stands out among all of these techniques since it is affordable, environmentally benign, produces less sludge, and has no hazardous consequences. In adsorption, the adsorbent's surface is covered with the adsorbate that will help to remove phenol ions from water or aqueous solution. Many diverse adsorbents are used for phenol removal, such as nickel oxide (Dehmani and Abouarnadasse, 2020), alumina (Li et al., 2017), Hematite (Dehmani et al., 2020), Calcined products of Mg–Al layered double hydroxides/single-walled carbon nanotubes (Zhang et al., 2019) etc. The remarkable effectiveness of oxides in eliminating organic contaminants from wastewater has been consistently demonstrated. Iron oxides, one of the most prevalent mineral groups on Earth, are among them and have shown to be helpful in a wide range of applications in both study and industry. Many people believe that these environmentally benign materials have a lot of potential for usage in a range of applications, particularly in magnetization, medical science, catalysis and environmental applications. Due to their superior adsorption affinity and capacity, quicker adsorption rate, and bigger surface areas when compared to other adsorbents they have interestingly shown tremendous promise as adsorbents for the removal of environment contamination (Ebrahim et al., 2016).

Iron oxides' structural and textural characteristics, as well as their precursors and precipitation agents, have a substantial impact on their activity. There has already been a significant amount of published research on the adsorption of organic molecules into the synthetic iron oxides. For instance, sarker et al. (Sarker and Fakhruddin, 2017) produced rice straw and investigated the possibility of phenol adsorption on it. Hematite (-Fe_2O_3), which effectively eliminates o-phthalic acid under a variety of environmental conditions, was created by Hwang et al (Hwang et al., 2007).

Presently, iron oxide and the derivatives of iron oxide with another adsorbent are extensively used for phenol removal of water from wastewater. Iron oxide is cheap and easily accessible and also has a high affinity than any other metal oxides. The surface area will increase with electrical, magnetic, and chemical properties during the elimination of phenol due to its nanoscale structure and size. The high cost of activated carbon and regeneration losses prompted a search for less expensive bio-adsorbent (Xu et al., 2012). In India, it is simple and common to obtain rice husk ash (RH). India is the second-largest producer of rice worldwide. Moreover, RH is waste from the manufacture of rice, which is used as cow feed and is likewise regarded as an efficient adsorbent (Mohamed et al., 2018).

Thorough literature search was done and to the best of our knowledge, fewer publications have been made about the RH+Fe used to remove phenol from wastewater. This study synthesised RH+Fe, and then used a scanning electron microscope (SEM), X-ray powder diffraction (XRD), Fourier-transform infrared spectroscopy (FTIR), and particle size analysis to thoroughly analyse its physicochemical qualities as an adsorbent. Several parameter tests looked at the effects of time, adsorbent dose, pH, and beginning concentration. Kinetic, thermodynamic, and isotherm studies were used to demonstrate the phenolic property of the RH+Fe adsorbent. The potential of an adsorbent was also discovered through the study of regeneration research.

II. MATERIALS AND METHODS

A. *Materials*

Ferrous chloride ($FeCl_2.4H_2O$, 98%), Ferric chloride ($FeCl_3.6H_2O$, 98%), sodium hydroxide (NaOH, AR 99%), and phenol (A.R. 98%) were procured from Merck. Rice husk was purchased from nearby rice mill. All of the substances were highly pure analytical reagents that were employed in the studies. Demineralized water was utilised for chemical preparations and testing in later research.

B. *Preparation of RH adsorbent*

RH was washed with 10 % HCL and kept in the oven for drying at 90 ºC for 20 h. After that RH was crushed and kept at 500 ºC in a muffel furnace for 8 h and form a white color powder. RH was sieved through 425 µm and washed five times with demineralized water and dried again in the oven at 60 ºC for 24 h.

C. *RH+Fe oxide Synthesis*

For RH+Fe NPs synthesis, co-precipitation technique was used. The NPs was synthesized using Ferric chloride (4 g), Ferrous chloride (4g) and RH (8 g) with HCL dissolved in demineralized water (200 mL) in a beaker at 90 ºC for 120 min for 8 h. The dropwise 1.5 M NaOH was added while stirring. Then the NPs was centrifuged at 2500 rpm for 20 min and separated in filter paper. Afterwards, the filter paper was kept in oven for 4 h at 90 ºC. Lastly, the powdered RH+Fe was obtained and stored in a small bottle.

D. *Batch adsorption experiments*

In this study, RH+Fe nanoparticles (NPs) adsorbent was employed in batch studies to optimise the parameters while phenol was assessed utilising the phenol assay process. Each experiment was carried out in a beaker containing 100 mL of phenol solution, and the required NPs quantities were agitated in an orbital shaker. Before filtering it via Whatman filter paper, the solution was agitated. Later, the filtered solution was evaluated using the APHA 23rd edition phenol assay technique. NaOH (0.1 M) and HCL (0.1 M) were employed in tests to modify the pH solution. Using equations (1) and (2), the effectiveness of phenol removal and adsorption capacity were assessed.

$$\%\text{Removalefficiency} = \frac{C_i - C_e}{C_i} \times 100 \quad (1)$$

$$q_e = \frac{(C_O - C_e)V}{m} \quad (2)$$

Whereas C_i and C_e represent initial and equilibrium concentrations of phenol in solution (g L^{-1}), V is the volume of the solution (L), and m is the mass of the adsorbent (g).

E. Characterization of RH+Fe adsorbent

For characterization, by using the KBr pellet method and FTIR spectroscopy (Nicolet 6700), the types of bonds present in the adsorbent were identified in the 400–4000 cm^{-1} range. An X-ray diffractometer (PAN analytical X'pert PRO) investigation uses Cu-K radiation (1.5406 Å) at an accelerating voltage of 40 kV and a current of 30 mA to identify the phases of the NPs. The morphology of the particle was subsequently determined using TEM on a JEM 2100 (Make: JEOL) microscope. Field Emission-Scanning Electron Microscope (FE-SEM) (Zeiss Ultra 55) was used to examine the adsorbent's morphology, size, and structure. The material was mixed in the solvent also coated with gold for examination. A Malvern 890 particle size analyzer made it possible to determine the NPs size.

III. RESULTS AND DISCUSSION

Later, to evaluate the amount of phenol removed from RH+Fe after and before adsorption (AD & BD), FTIR was used, as shown in Fig. 2. RH+Fe research on BD and AD shows no distinctions between the two. The pure Fe spectrum, which is present at 557 cm-1, is due to vibrations peculiar to the Fe-O bond. SiO2 was discovered at 879 cm-1. The peaks at 1627 cm-1, 1429 cm-1, and 2360 cm-1 additionally indicate the O-H, CH3, C=C, and C-H bonds. Assignments for frequency and position were shown in Table 1 (Ouallal et al., 2019).

Further, the characteristic diffraction peak in RH+Fe AD and BD was identified using an X-ray diffractometer, as shown in Fig. 3. The peaks were attributed to the Joint Committee on Powder Diffraction Standards (JCPDS) X-ray data file of Fe (39-1346). Patterns of RH+Fe were 22.0°, 25.2°, 27.1°, 30.0°, 32.1°, 38.4°, 44.2°, 57.2°, and 63.0° at its peak value of 2Θ, which corresponds to the peak (004), (420), (151), (220), (600), (311,040), (222), (110), (422), (511), and (440). While the peak of Fe-O was apparent at 30.0°, the peak of SiO_2 is seen in the conspicuous peaks at 35.4°. The prominent peak of the adsorbent indicates the crystalline nature of the materials. Using the Debye-Scherer equation, it was found that the average crystallite size of these NPs was 55.7 nm, where h is the Bragg angle, K is the Debye-Scherer constant (0.9), β is the full width at half maximum of the biggest peak, and is the X-ray wavelength close to 1.5406 Å (in radians). As a result, the XRD results confirmed that RH+Fe was produced by synthesis process (Morjène et al., 2021). Later on, in Fig 4 the SEM analysis shows the flower-type image of indicate the adsorption of RH in Fe. The colloidal formation indicates the Fe NPs was prepared. Magnetic property helps the iron oxide NPs to attract phenol which helps in removal of aqueous solution. While EDX analysis was confirmed the elemental composition showing 48 % of iron, 23 % of RH and 29 % of oxygen which is an indication for successful formation of material (Sathya Priya and Sureshkumar, 2020).

For RH+Fe NPs, The particle dispersion was determined using a particle size analyzer, as shown in Fig. 5. The average size of the adsorbent is 78 nm. The conjoining of NP makes the size of the adsorbent important (Kong et al., 2020).

A. Different Parameters Analysis

1) Effect of Dosage, contact time, concentration, and pH

At a constant temperature of 50° C and 200 rpm of stirring, batch investigations of adsorbent dosage for RH+Fe adsorbent for defluoridation were carried out. It was clear from Fig. 6 that the removal efficiency of the Phenol trend line rose from 0.1 to 3 g L^{-1} but remained constant at 2.6 g L^{-1}. The availability of a broad surface area and additional adsorption sites with increasing adsorbent dosage causes the removal efficiency to increase. Due to the overlapping of active sites at higher dosages and the absence of holes in the adsorbent's active surface area, the adsorption remains constant. The process of surface adsorption depended heavily on the volume of micropores and the accessibility of a definite surface area. On RH+Fe adsorbent, the highest Phenol adsorption was 96 % at 84 mg g^{-1} adsorption capacity (Ma et al., 2018).

In a batch experiment, the Phenol removal effectiveness was demonstrated by maintaining a dose of 2.6 g L^{-1} at a temperature of 50° C and stirring at a velocity of 200 rpm, as shown in Fig. 7. When the RH+Fe was utilized for Phenol adsorption, the removal effectiveness of the Phenol increased up to 60 min, reaching 96 %, and then remained steady until 90 min, where adsorption capacity reaches to 84 mg g^{-1}. This trend can be caused by the porous structure's maximal active sites for adsorption with the passage of time and the surface area's high surface area. Additionally, as time passes, the adsorption stays constant since an oxidant is no longer available for adsorption. Two crucial mechanisms contributed to the decline in Phenol adsorption; one was the diffusion phenomenon which occurs among the pores and active surface area in the adsorbent.

Another argument was made when the Phenolate ions were adsorbed on the surface sites, and the repulsion was produced between Phenol and the adsorbent (Nath et al., 2013). The concentration was examined with constants such as a dosage of 2.6 g L^{-1}, temperature 50 °C, stirring rate 200 rpm, and time 60 min for the RH+Fe adsorbent in a batch experiment between 10 mg L^{-1} and 100 mg L^{-1} shown in Fig. 8. The elimination of Phenol increases significantly in 10 mg L^{-1} with 96 % removal efficiency and 85 mg g^{-1} adsorbent capacity, according to the study. Due to additional binding sites being available at a lower concentration, the initial concentration then rises. Due to active sites saturation, reduced mass transfer, and a shortage of binding sites for Phenol adsorption, adsorption reduces at increasing concentrations. Later, the experimental Phenol adsorption data were identified and presented below using isotherms and kinetic model (Hasan and Jhung, 2015). The pH of an aqueous solution is the most important element in determining how ions are adopted on the surface of an oxide. In experiments conducted in the pH range of 2-12 with a dose of 2.6 g L^{-1} at a temperature of 50 °C, stirring rate of 200 rpm, and a duration of 60 min, the interaction of the Phenolate ion and the RH+Fe was focused on pH. The adsorption capacity of Phenol was shown to increase with initial pH value and gradually decline with higher pH. This cause under the interfacial attraction on the adsorption properties of phenol. The higher pH is at 6 due to the strong π- π interaction and H-bond interaction between the adsorbent and phenol. At higher pH the decrement in adsorption is due to homogenous charge repulsion between the phenolates and negatively charge RH+Fe. As a result, for the RH+FeNPs, the maximum adsorption capacity was attained 96 % removal efficiency at 6 pH and 84 mg g^{-1} adsorbent capacity as shown in Fig 9 (Mandal et al., 2019).

2) Adsorption Kinetics

The experimental data were fitted to kinetic models such as the pseudo-first order, and pseudo-second order was followed to better describe the potential adsorption, mechanism of Phenol on the adsorbent, and the correlative parameters. The eq. (6 & 7) are displayed below.

$$\log(q_e - q_t) = \log q_e - \frac{k_1 t}{2.303} \quad (6)$$

$$\frac{t}{q_t} = \frac{1}{k_2 q_e^2} + \frac{t}{q_e} \quad (7)$$

The fitted kinetic model is shown in Fig. 10, and all the data are shown in Table 2. The eq. (6). is pseudo first order where qe and qt denote the amount of Phenol adsorbed (mg g^{-1}) at equilibrium and at time t, respectively. K_f (min^{-1}) is the rate constant of pseudo-first-order adsorption reaction. The eq.(7) shows pseudo-second- order reaction where Ks is the rate constant for the pseudo-second-order reaction (g mg^{-1} min^{-1}). q_e and q_t are the amounts of solute adsorbed at equilibrium and at any time t (mg g^{-1}) (Zhang et al., 2015).

The correlation coefficient R^2 was discovered to be the most significant and been made best match by experimental data. Among these two pseudo-second order (R^2 = 0.96), provided the best explanation for the kinetic data. Thus, chemical interactions i.e., chemisorption phenomena relating valency forces through sharing or exchange of electrons between sorbent and sorbate, were the rate-limiting step (Liu et al., 2010). The standard deviation (sd) was used to evaluate the kinetic models that were used to match the sorption data. In Pseudo first order model, smaller sd values show that Phenol adsorption is dependent on the active sites on RH+Fe composite.

3) Adsorption Isotherms

The feasibility of the reaction, the interface between the Phenol and RH+Fe adsorbent, the adsorption characteristics, the peripheral phenomena of the NPs, and the equilibrium data were all examined using isotherms. The investigational data from Langmuir and Freundlich were examined in this work along with varying beginning concentrations (10-100 mg L^{-1}) with 2.6 g L^{-1} dosage of RH+Fe adsorbent, as shown in Table 3 and Fig. 11.

The Langmuir isotherm presupposes either monolayer adsorption or uniform dispersion of the adsorbent with a restricted number of identical sites on homogeneous surfaces. For the RH+Fe adsorbent had an adsorption capacity of 90 mg g^{-1}, and the graph was plotted with Ce/qe and qe and R^2 0.96 (Wen et al., 2015).

$$\frac{C_e}{Q_e} = \frac{1}{q_m b} + \frac{C_e}{q_m} \quad (8)$$

The equation was stated in eq. (8) where, Q_e is the equilibrium amount of adsorbate in adsorbent (mg g^{-1}), C_e is the equilibrium concentration capacity (mg L^{-1}), q_m is the maximum Phenol adsorption capacity (mg g^{-1}), and b is the isotherm constant (mg L^{-1}).
When it comes to multilayer adsorption in the Freundlich isotherm, the non-ideal and reversible adsorption is characterised by heterogeneous surfaces and an uneven distribution of adsorption sites. The graph, of log Q_e and log C_e was plotted, shows Phenol adsorption on RH+Fe in Fig. 11b and provides values of K_f and 1/n with R^2 0.95 (Hasan and Jhung, 2015).

$$\log Q_e = \log K_f + \frac{1}{n}\log C_e \quad (9)$$

The equation was stated in eq. (9), where K_f = Freundlich equilibrium constant (L g^{-1}), and 1/n = constant related to energy of adsorption intensity in a heterogeneous system.
The experimental and estimated value were resolute, together with R^2, to assess best-fitting isotherm. Table 3 displays the R^2 value. In comparison to Langmuir and Freundlich, Langmuir have a higher R^2 value. Due to the establishment of an ionic and covalent link between Phenol and RH+Fe, monolayer adsorption and homogenous surface will be implied according to Langmuir theory. Additionally, the Freundlich isotherms fall between 1 and 10, indicating that the Phenol was readily adsorbed on the adsorbent's surface. Table 4 compares several adsorbents based on their capacity for adsorption.

4) Thermodynamics Study

The results of the investigation into how temperature affects the phenol's adsorption to the RH+Fe are displayed in Fig. 12. The temperature optimisation and plot of T^{-1} vs. lnK were shown in Fig. 12(a) & (b). The adsorption process and its possibilities were examined in the thermodynamic process. Using Fig. (12b), the standard enthalpy (ΔH^o) and standard entropy (ΔS^o) change, as well as the intercept and slope, were calculated. The difference in Gibbs free energy (ΔG^o) was calculated using eq. (10–12). The outcome is displayed in Table 5. The phenol adsorption rises with temperature. The adsorption has a more significant cause, which is why the reaction adheres to the La Chattelier principle. The value of (ΔG^o) increases as the temperature increases. This proves that the adsorption occurred on its own. The increased randomness at the solid-liquid interface is shown to increase as the number of species increases by the positive value of the (ΔS^o). When phenol and a solid surface come into touch, water molecules are released. The (ΔH^o) value denotes the type of physical adsorption that is occurring in the system, which is surface adsorption of RH+Fe. By a positive (ΔH^o) result, the endothermic adsorption is verified (Warmadewanthi and Liu, 2009). As a result, in the present investigation, higher temperatures were preferred than lower temperature.

$$\Delta G^\circ = RT\ \ln K_C \quad (10)$$

$$\Delta G^\circ = \Delta H^\circ - T\Delta S^\circ \quad (11)$$

$$\log\left(\frac{q_e m}{C_e}\right) = \frac{\Delta S^\circ}{2.303R} + \frac{-\Delta H^\circ}{2.303RT} \quad (12)$$

Where R= universal gas constant (8.314 J mol^{-1} K^{-1}), and Kc = adsorption distribution coefficient.

5) Recyclability Study

Reusability is a key factor to take into account when considering whether to employ an adsorbent practically for commercial reasons. The investigation was conducted using batch experiments, and the graph is shown in Fig. 13. Following that, 0.1 M NaOH was used to stir the used adsorbent solution for 2 h. After centrifuging, the adsorbent was baked for 8 h at 90º C. Aiming all stages, recycled adsorbent was applied once more under identical conditions with a starting concentration of 10 mg L^{-1}. The fifth cycle, which is depicted in Fig. 13, produced phenol with an efficiency of 82 %. Efficiency declines as a result of patches on the adsorbent's surface becoming inaccessible. The results showed that the adsorbent that had been treated with NaOH could regenerate and be reused quickly, proving that the material was effective, affordable, and environmentally friendly with amazing reusability and its true application potential (Cheng and Zheng, 2014).

IV. CONCLUSIONS

The RH+Fe adsorbent was used in the current work to achieve phenol efficiency. The characterisation demonstrates that the RH+Fe adsorbent was expertly made. The ideal parameters were concentration10 mg L^{-1}, dosage 2.6 g L^{-1}, pH 6, and time 60 min, with a 96 % phenol elimination efficiency.

The adsorption of phenol and RH+Fe was largely dependent on optimised parameters. The RH+Fe adsorbent data was best suited to the Langmuir isotherm and had an adsorption capacity of 90 mg g^{-1}, which is monolayer adsorption between adsorbate and adsorbent, according to calculations made from the equilibrium data. The regeneration of phenol elimination indicated 82 % in the fifth stage. As a result, this study significantly advances our knowledge of viable and useful methods for removing phenol from adsorbents.

Data availability: All data generated or analysed during this study are included in this article. Any other datasets used during the current study are available from the corresponding author on reasonable request.

Compliance with ethical standards

Ethics approval: Not applicable.

Consent to participate: Consent.

Consent for publication: Consent.

REFERENCES

[1] Ahmadi, S; Igwegbe, C. A.: Adsorptive removal of phenol and aniline by modified bentonite: adsorption isotherm and kinetics study. Appl. Water. Sci. 8, 1–8 (2018). https://doi.org/10.1007/s13201-018-0826-3

[2] Cheng, G; Zheng, S. Y.: Construction of a high-performance magnetic enzyme nanosystem for rapid tryptic digestion. Sci. Rep. 4, 6947 (2014). https://doi.org/10.1038/srep06947

[3] Dehmani, Y.; Abouarnadasse, S.: Study of the adsorbent properties of nickel oxide for phenol depollution. Arab. J. Chem. 13, 5312–5325 (2020). https://doi.org/10.1016/j.arabjc.2020.03.010

[4] Dehmani, Y.; Alrashdi, A. A.; Lgaz, H.; Lamhasni, T.; Abouarnadasse, S.; Chung, I. M.: Removal of phenol from aqueous solution by adsorption onto hematite (α-Fe2O3): Mechanism exploration from both experimental and theoretical studies. Arab. J. Chem. 13, 5474–5486 (2020). https://doi.org/10.1016/j.arabjc.2020.03.026

[5] Dong, R.; Chen, D.; Li, N.; Xu, Q.; Li, H.; He, J.; Lu, J.: Removal of phenol from aqueous solution using acid-modified Pseudomonas putida-sepiolite/ZIF-8 bio-nanocomposites. Chemosphere. 239, 124708 (2020). https://doi.org/10.1016/j.chemosphere.2019.124708

[6] Ebrahim, S. E.; Sulaymon, A. H.; Saad Alhares, H.: Competitive removal of Cu2+, Cd2+, Zn2+, and Ni2+ ions onto iron oxide nanoparticles from wastewater. Desalin. Water. Treat. 57, 20915–20929 (2016). https://doi.org/10.1080/19443994.2015.1112310

[7] Ge, M.; Wang, X.; Du.; M, Liang, G.; Hu, G.; Alam, S. M. J.: Adsorption analyses of phenol from aqueous solutions using magadiite modified with organo-functional groups: Kinetic and equilibrium studies. Materials. 12, 96 (2018). https://doi.org/10.3390/ma12010096

[8] Hasan, Z.; Jhung, S. H.: Removal of hazardous organics from water using metal-organic frameworks (MOFs): Plausible mechanisms for selective adsorptions. J. Hazard. Mater. 283, 329–339 (2015). https://doi.org/10.1016/j.jhazmat.2014.09.046

[9] Hwang, Y. S.; Liu, J.; Lenhart, J. J.; Hadad, C. M.: Surface complexes of phthalic acid at the hematite/water interface. J. Colloid Interface Sci. 307,124–134 (2007). https://doi.org/10.1016/j.jcis.2006.11.020

[10] Kong, X.; Gao, H.; Song, X.; Deng, Y.; Zhang, Y.: Adsorption of phenol on porous carbon from Toona sinensis leaves and its mechanism. Chem. Phys. Lett. 739, 137046 (2020). https://doi.org/10.1016/j.cplett.2019.137046

[11] Li, S.; Wang, W.; Liang, F.; Zhang, W. X.: Heavy metal removal using nanoscale zero-valent iron (nZVI): Theory and application. J. Hazard Mater. 322, 163–171 (2017). https://doi.org/10.1016/j.jhazmat.2016.01.032

[12] Liu, Y. L.; Chang. Y.; Chang, Y. H.; Shih, Y. J.: Preparation of amphiphilic polymer-functionalized carbon nanotubes for low-protein-adsorption surfaces and protein-resistant membranes. ACS Appl Mater Interfaces 2, 3642–3647 (2010). https://doi.org/10.1021/am100811q

[13] Ma, Q.; Cui, L.; Zhou, S.; Li, Y.; Shi, W.; Ai, S.: Iron nanoparticles in situ encapsulated in lignin-derived hydrochar as an effective catalyst for phenol removal. Environ. Sci. Pollut. Res. 25, 20833–20840 (2018). https://doi.org/10.1007/s11356-018-2285-7

[14] Mandal, A.; Mukhopadhyay, P.; Das, S. K.: The study of adsorption efficiency of rice husk ash for removal of phenol from wastewater with low initial phenol concentration. SN Appl. Sci. 1, 1–13 (2019). https://doi.org/10.1007/s42452-019-0203-3

[15] Mehmanravesh, S.; Farhadi, K.; Torabian, A.; Hessam Hassani, A.; Fe3O4@GO on silica sand as an efficient and economical adsorbent; Typical application for removal of phenol and 2,4-dichlorophenol from water samples. Water. Environ. Res. 91, 1509–1517 (2019). https://doi.org/10.1002/wer.1146

[16] Mohamed, M.; Yusup, S.; Quitain, A. T.; Kida, T.: Utilization of rice husk to enhance calcium oxide-based sorbent prepared from waste cockle shells for cyclic CO2 capture in high-temperature condition. Environ. Sci. Pollut. Res. 1–15 (2018). https://doi.org/10.1007/s11356-018-2549-2

[17] Morjène, L.; Aloulou, F.; Tasbihi, M.; Schwarze, M.; Schomäcker, R.; Seffen, M.: New composite material based on Kaolinite, cement, TiO2 for efficient removal of phenol by photocatalysis. Environ. Sci. Pollut. Res. 28, 35991–36003 (2021). https://doi.org/10.1007/s11356-021-13150-y

[18] Nath, K.; Panchani, S.; Bhakhar, M. S.; Chatrola, S.; Preparation of activated carbon from dried pods of Prosopis cineraria with zinc chloride activation for the removal of phenol. Environ Sci. Pollut. Res. 20, 4030–4045 (2013). https://doi.org/10.1007/s11356-012-1325-y

[19] Ouallal, H.; Dehmani, Y.; Moussout, H.; Messaoudi, L.; Azrour, M.; Kinetic, isotherm and mechanism investigations of the removal of phenols from water by raw and calcined clays. Heliyon. 5, 1616 (2019). https://doi.org/10.1016/j.heliyon.2019.e01616

[20] Sarker, N.; Fakhruddin, A. N. M.: Removal of phenol from aqueous solution using rice straw as adsorbent. Appl. Water. Sci. 7, 1459–1465 (2017). https://doi.org/10.1007/s13201-015-0324-9

[21] Sathya Priya D, Sureshkumar, M. V.: Synthesis of Borassus flabellifer fruit husk activated carbon filter for phenol removal from wastewater. Int. J. Environ. Sci. Technol. 17, 829–842 (2020). https://doi.org/10.1007/s13762-019-02325-3

[22] Warmadewanthi, B.; Liu, J. C.: Selective separation of phosphate and fluoride from semiconductor wastewater. Water. Sci. Technol. 59, 2047–2053 (2009). https://doi.org/10.2166/wst.2009.157

[23] Wen, S.; Wang, Y., Dong, S.: Performance and characteristics of fluoride adsorption using nanomagnetite graphite-La adsorbent. RSC Adv. 5, 89594–89602 (2015). https://doi.org/10.1039/c5ra15215af

[24] Xu, P.; Zeng, G. M.; Huang, D. L.; Feng, C. L.; Hu, S.; Zhao, M. H.; Lai, C.; Wei, Z.; Huang, C.; Xie, G. X.; Liu, Z. F.: Use of iron oxide nanomaterials in wastewater treatment: A review. Sci. Total Environ. 424, 1–10 (2012). https://doi.org/10.1016/j.scitotenv.2012.02.023

[25] Zhang, X.; Zhang, S.; Yang, H.; Shao, J.; Chen, Y.; Feng, Y.; Wang, X.; Chen, H.: High temperature ammonia modification of rice husk char to enhance CO_2 adsorption: Influence of pre-deashing. RSC Adv. 5, 106280–106288 (2015). https://doi.org/10.1039/c5ra23365h

[26] Zhang, Z.; Sun, D.; Li, G.; Zhang, Bo.; Zhang, Bei Qiu S.; Li, Y.; Wu, T.: Calcined products of Mg–Al layered double hydroxides/single-walled carbon nanotubes nanocomposites for expeditious removal of phenol and 4-chlorophenol from aqueous solutions. Colloids Surfaces A Physicochem. Eng. Asp. 565, 143–153 (2019). https://doi.org/10.1016/j.colsurfa.2019.01.001

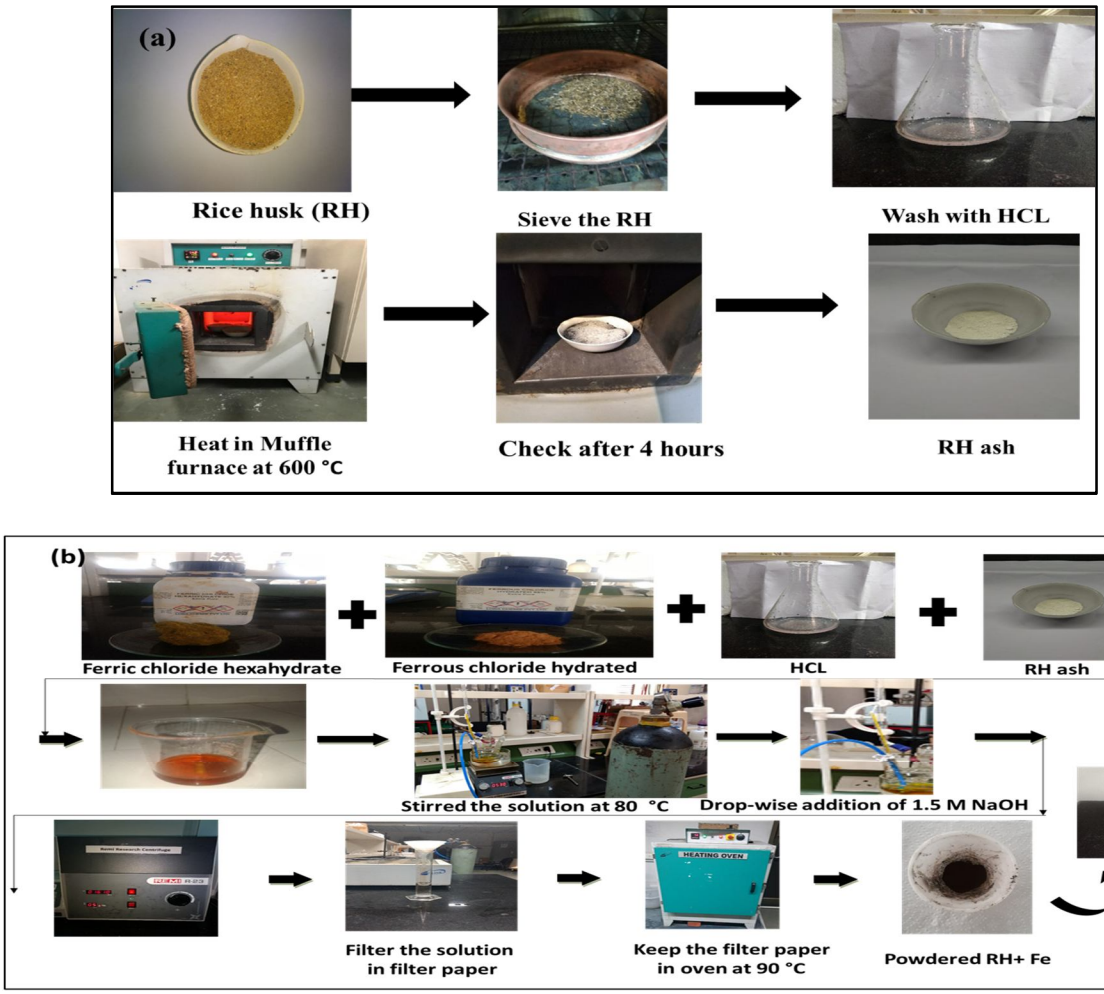

Fig 1. Synthesis process of adsorbent which were done in lab

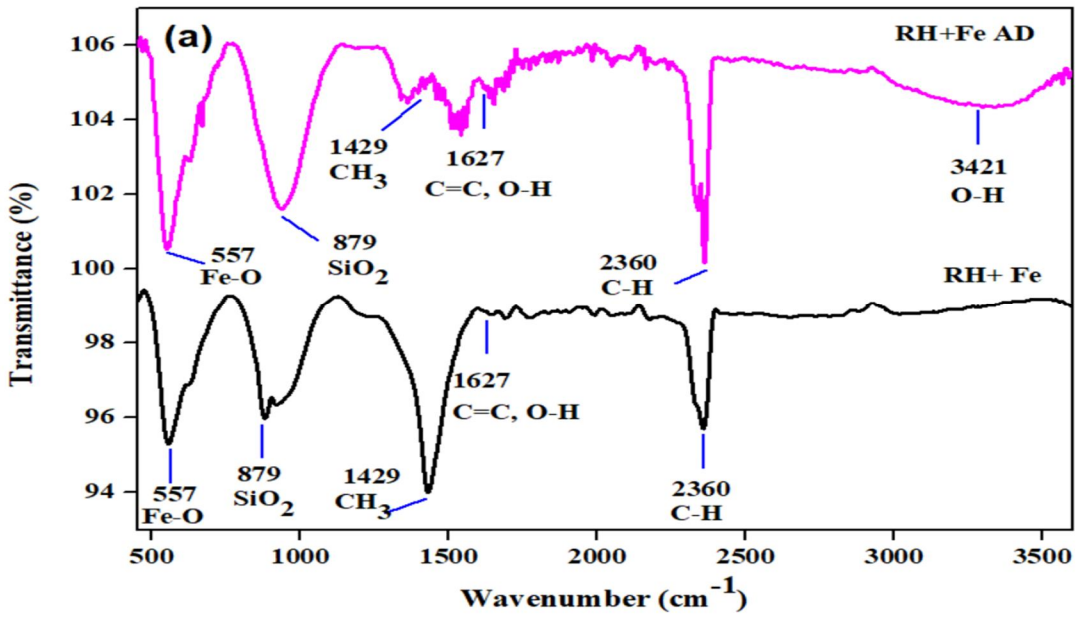

Fig 2. FTIR spectra of adsorbent

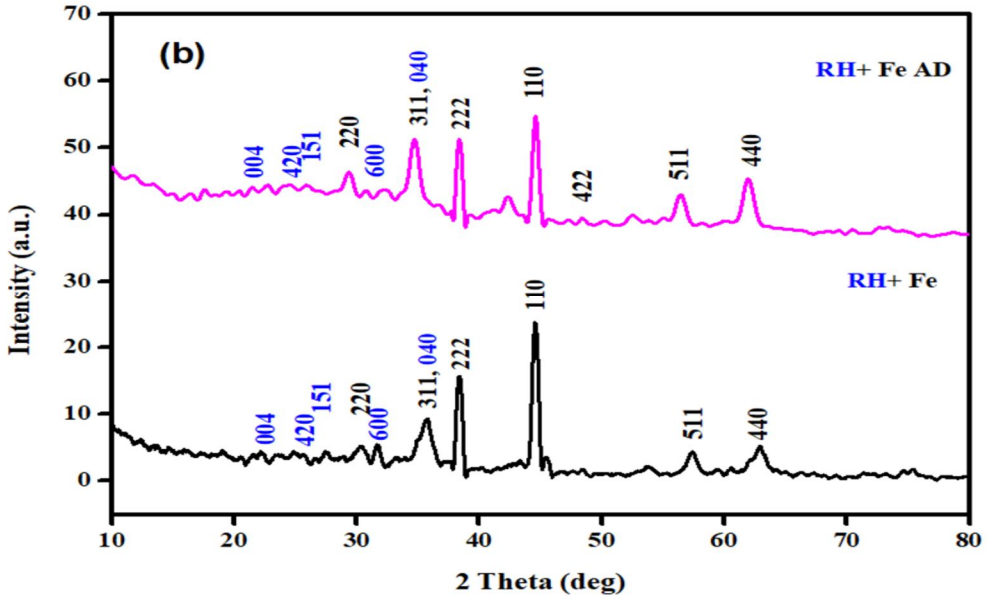

Fig 3. XRD of adsorbent

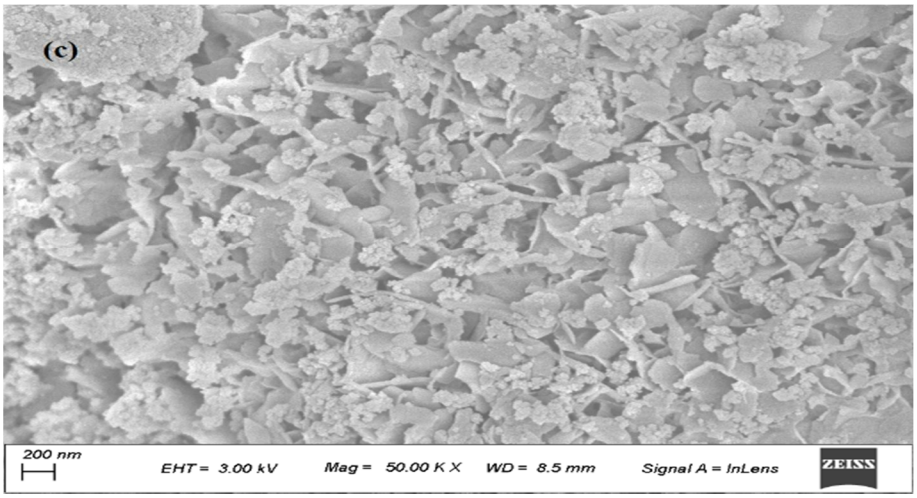

Fig 4. (a) SEM of adsorbent

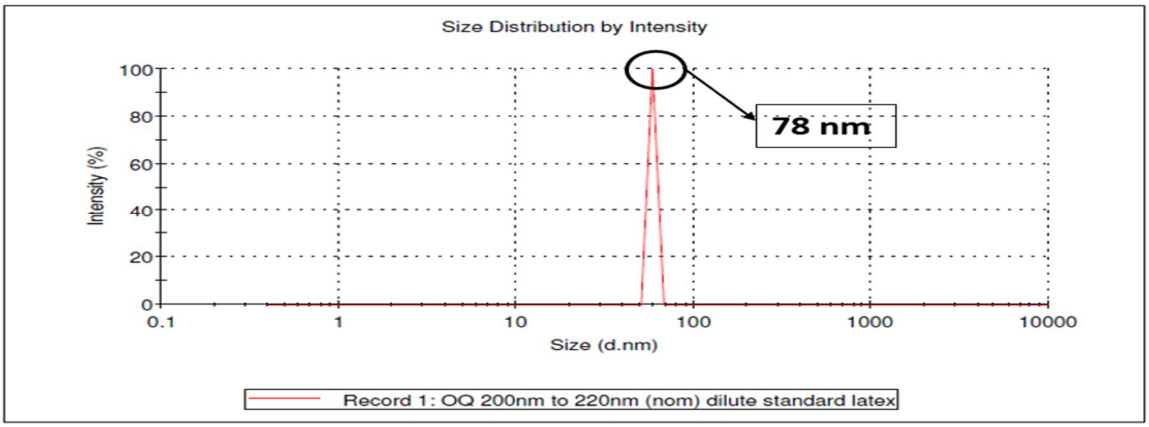

Fig 5. Particle size analysis of adsorbent

ISSN: 2321-9653; IC Value: 45.98; SJ Impact Factor: 7.538
Volume 13 Issue II Feb 2025- Available at www.ijraset.com

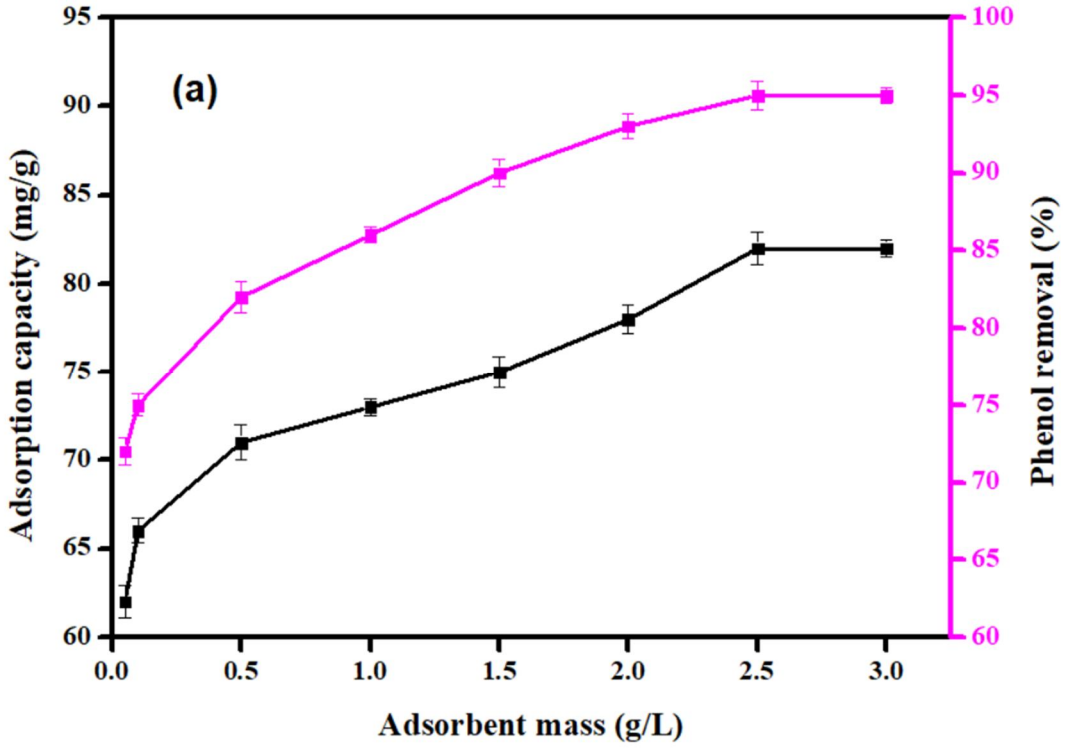

Fig 6. Effect of dosage of adsorbent (C_0: 10 mg/L, Contact time: 60 min, T: 50 ºC, Agitation speed: 200 rpm, pH: 6)

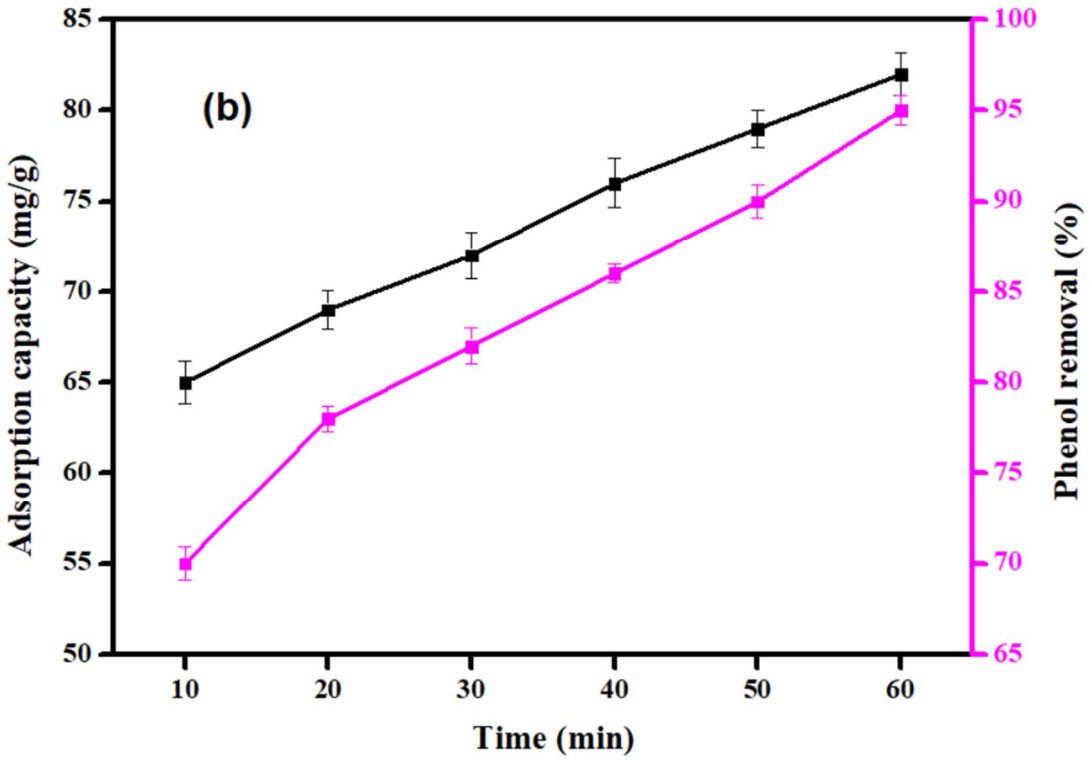

Fig 7. Effect of time of adsorbent (C_0: 10 mg/L, Adsorbent dosage: 2.5 g/L, T: 50 ºC, Agitation speed: 200 rpm, pH: 6)

ISSN: 2321-9653; IC Value: 45.98; SJ Impact Factor: 7.538
Volume 13 Issue II Feb 2025- Available at www.ijraset.com

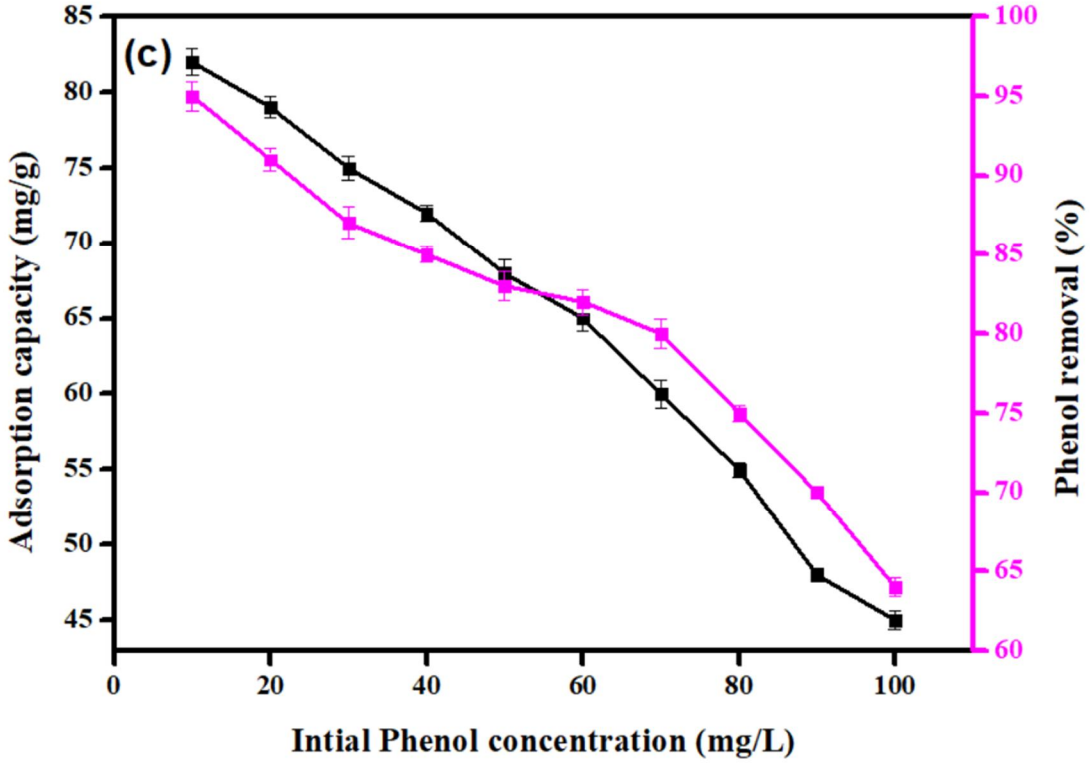

Fig 8. Effect of the initial concentration of adsorbent (Adsorbent dosage: 2.5 g/L, Contact time: 60 min, T: 50 ºC, Agitation speed: 200 rpm, pH: 6)

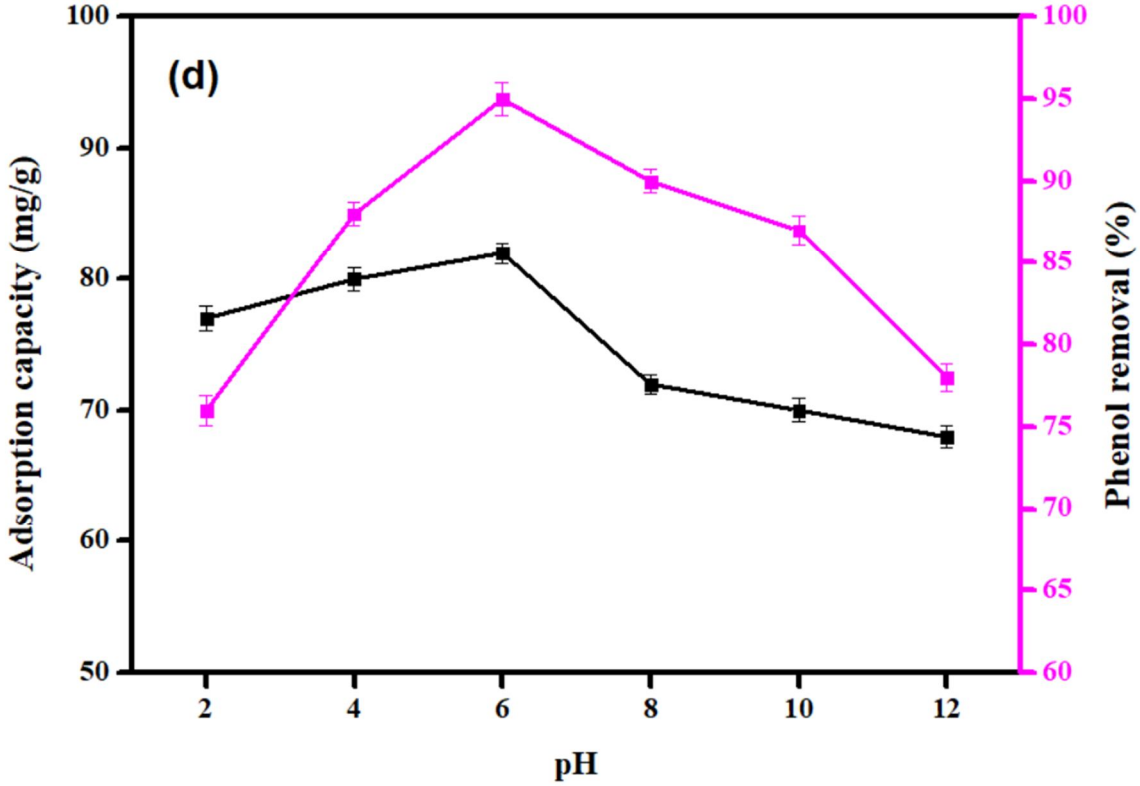

Fig 9. Effect of pH of adsorbent (Adsorbent dosage: 2.5 g/L, Contact time: 60 min, T: 50 ºC, Agitation speed: 200 rpm, C_0: 10 mg/L)

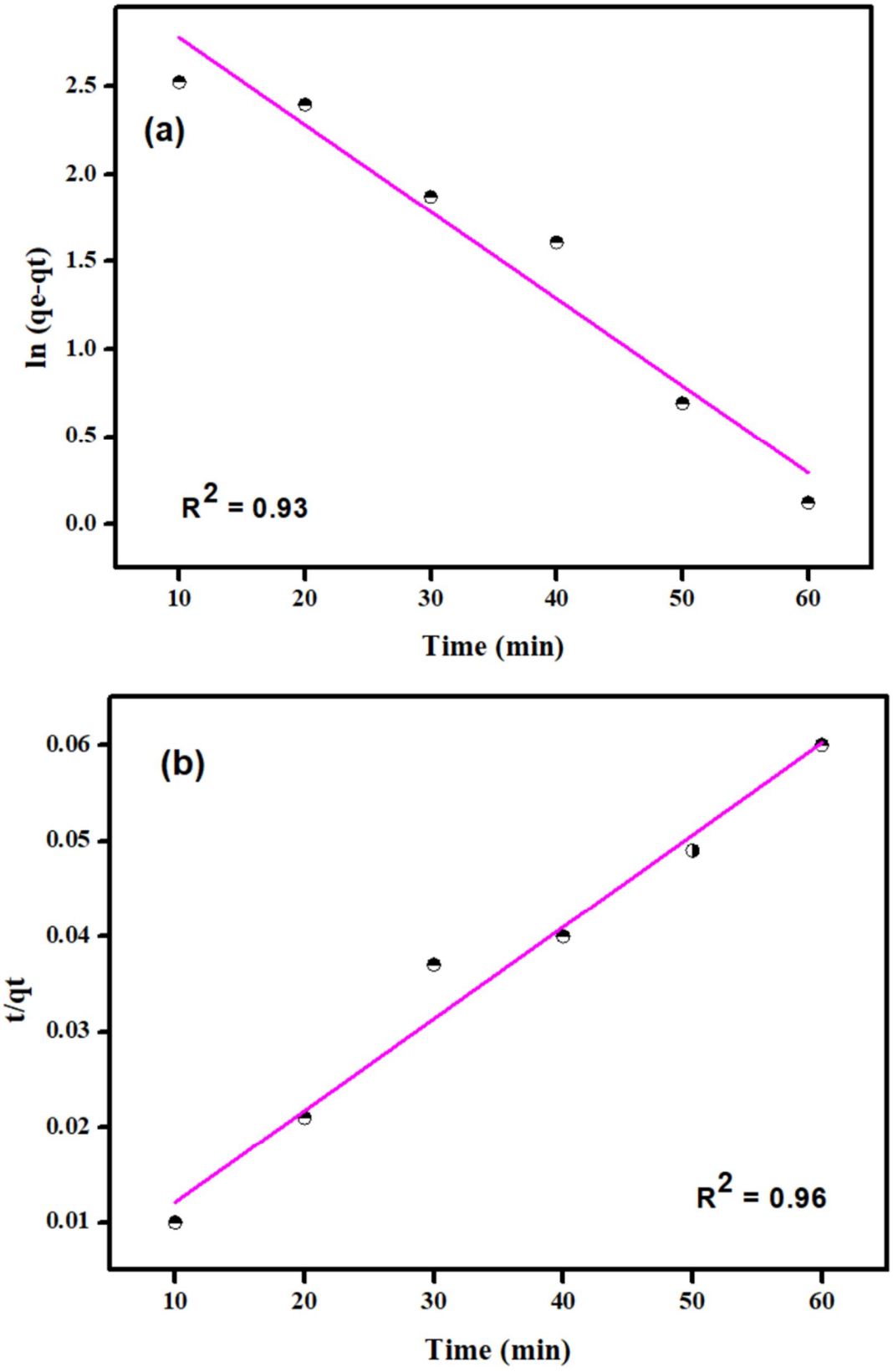

Fig 10. Kinetic study (a) pseudo-first-order (b) pseudo-second-order

ISSN: 2321-9653; IC Value: 45.98; SJ Impact Factor: 7.538
Volume 13 Issue II Feb 2025- Available at www.ijraset.com

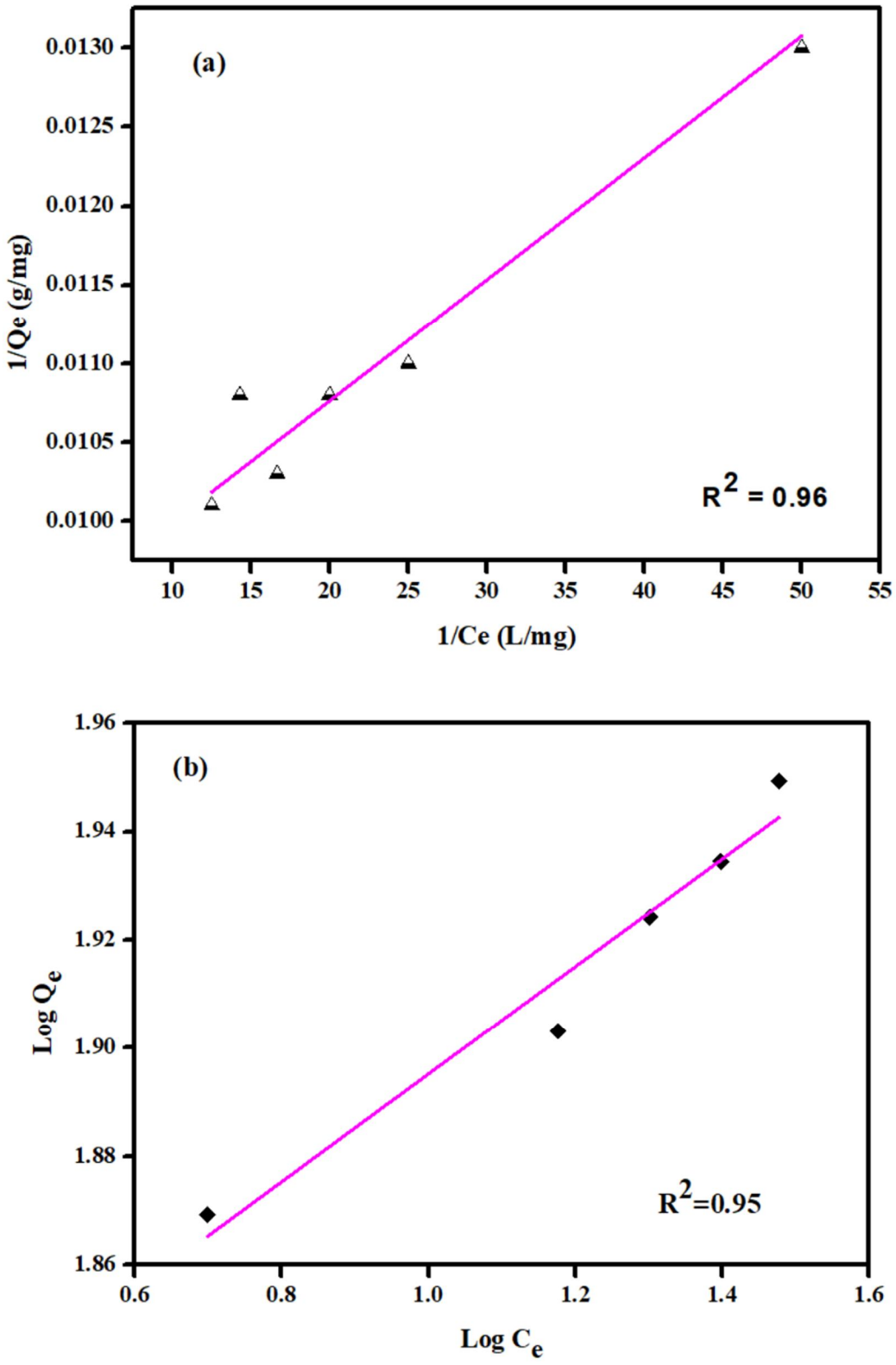

Fig 11. Isotherm study (a) Langmuir (b) Freundlich

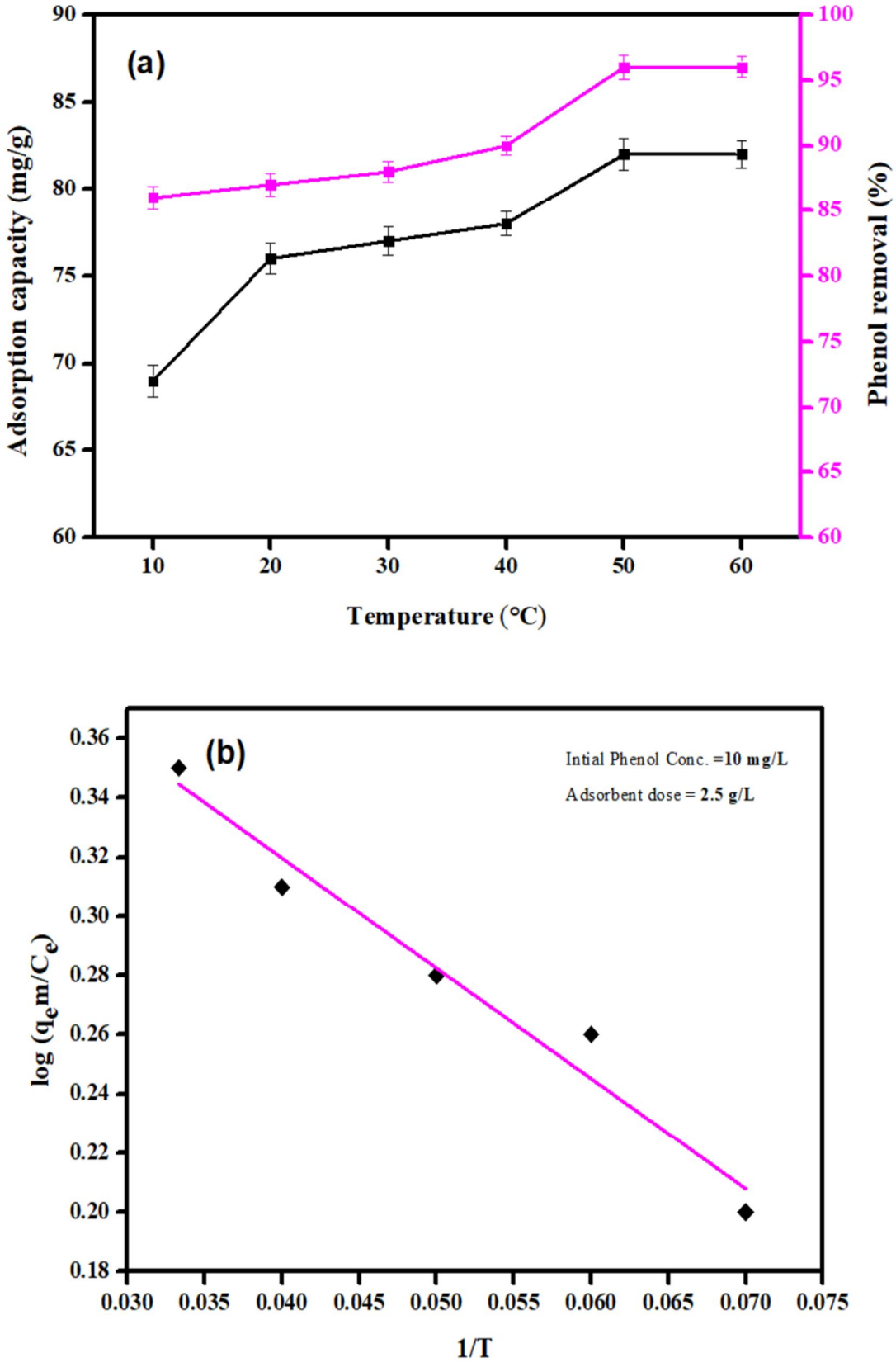

Fig 12. (a) Temperature study (b) Thermodynamic study

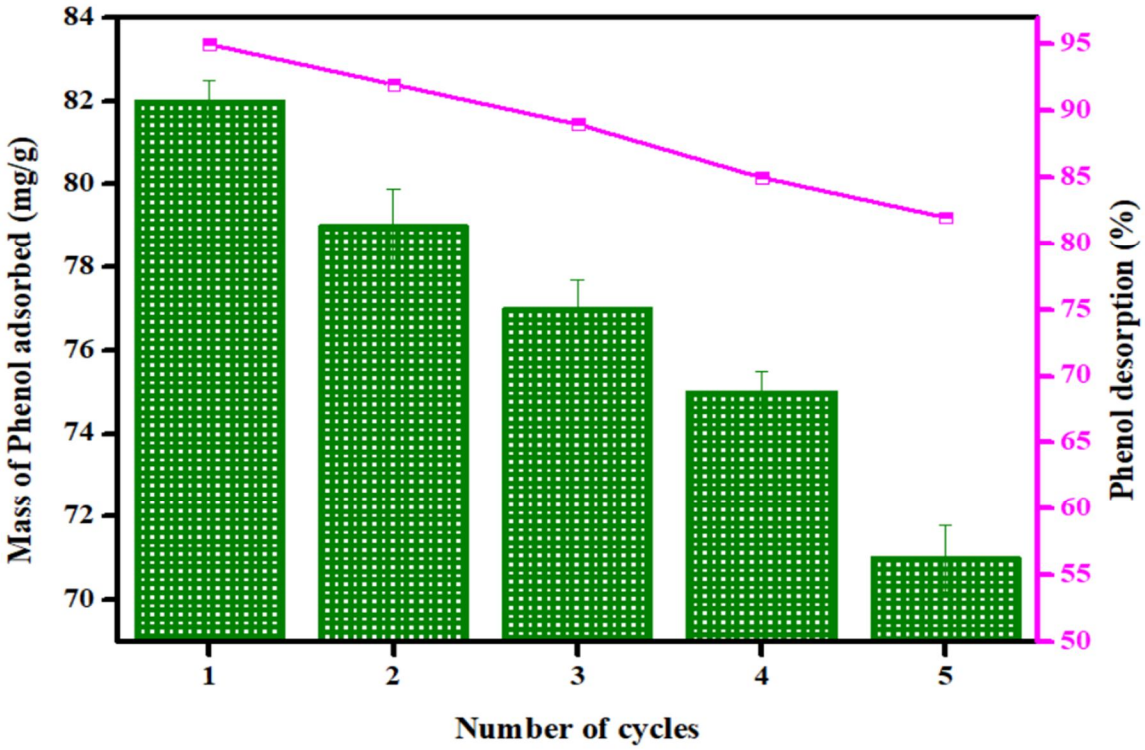

Fig 13. Regeneration study (Adsorbent dose: 2.5 g/L, Contact time: 60 min, T: 50 ºC, Agitation speed: 200 rpm, pH: 7)

Table 1. FTIR table for RH+Fe adsorbent.

Frequency cm^{-1}.	Position assignment
557	Fe-O
879	SiO_2
1627	O-H
1627	C=C
1429	CH_3
2360	C-H

Table 2. Kinetic constants and correlation coefficient.

Pseudo first order				Pseudo-second-order kinetic		
$q_{e,\ expt}$ (mg/L)	$q_{e,cal}$ (mg/L)	k_1 (1/min)	R^2	$q_{e,cal}$ (mg/L)	k_1 (mg/g.min)	R^2
3	1	1.8	0.93	2	0.09	0.96

Table 3. Isotherms study for Phenol adsorption

Langmuir isotherm		Freundlich isotherm	
q_m	90	K_f	9
b	7	N	1.3
R^2	0.96	R^2	0.95

ISSN: 2321-9653; IC Value: 45.98; SJ Impact Factor: 7.538
Volume 13 Issue II Feb 2025- Available at www.ijraset.com

Table 4. Comparison study of different adsorbent with adsorption capacity.

Adsorbent	pH	Adsorption capacity (mg/g)	References
α-Fe_2O_3	2-5	16.17	(Dehmani et al., 2020)
Iron impregnated A/C	>7	2.0	(Ge et al., 2018)
Acid modified bentonite	4	6.8	(Ahmadi and Igwegbe, 2018)
Rice husk	7.61	7.89	(Mandal et al., 2019)
Microorganism P. putida and acid-modified CESEP/ZIF-8	-	5.96	(Dong et al., 2020)
Borassus flabellifer fruit husk activated carbon (H_2SO_4 activation)	2	13.42	(Sathya Priya and Sureshkumar, 2020)
Fe_3O_4@GO on silica sand	5	13.97	(Mehmanravesh et al., 2019)
RH+Fe	6	90	Present study

Table 5. Thermodynamic properties phenol adsorption at different temperature

Temperature (ºC)	ΔH° (kJ/mol)	ΔS° (kJ/mol)	Ea (KJ /mol)	-ΔG° (KJ/mol)
30	2.9	1.6	1.52	145.2
40				224.6
50				544.5

Highlights

- RH+Fe NPs acts as an excellent adsorbent for phenol adsorption because of ion exchange and electrostatic attraction mechanism.
- Phenol removal efficiency was achieved 96 % with 60 min by RH+Fe NPs.
- Phenol removal parameters on RH+Fe NPs have been optimized.
- Regeneration study showed 82 % removal efficiency till 5^{th} cycle.

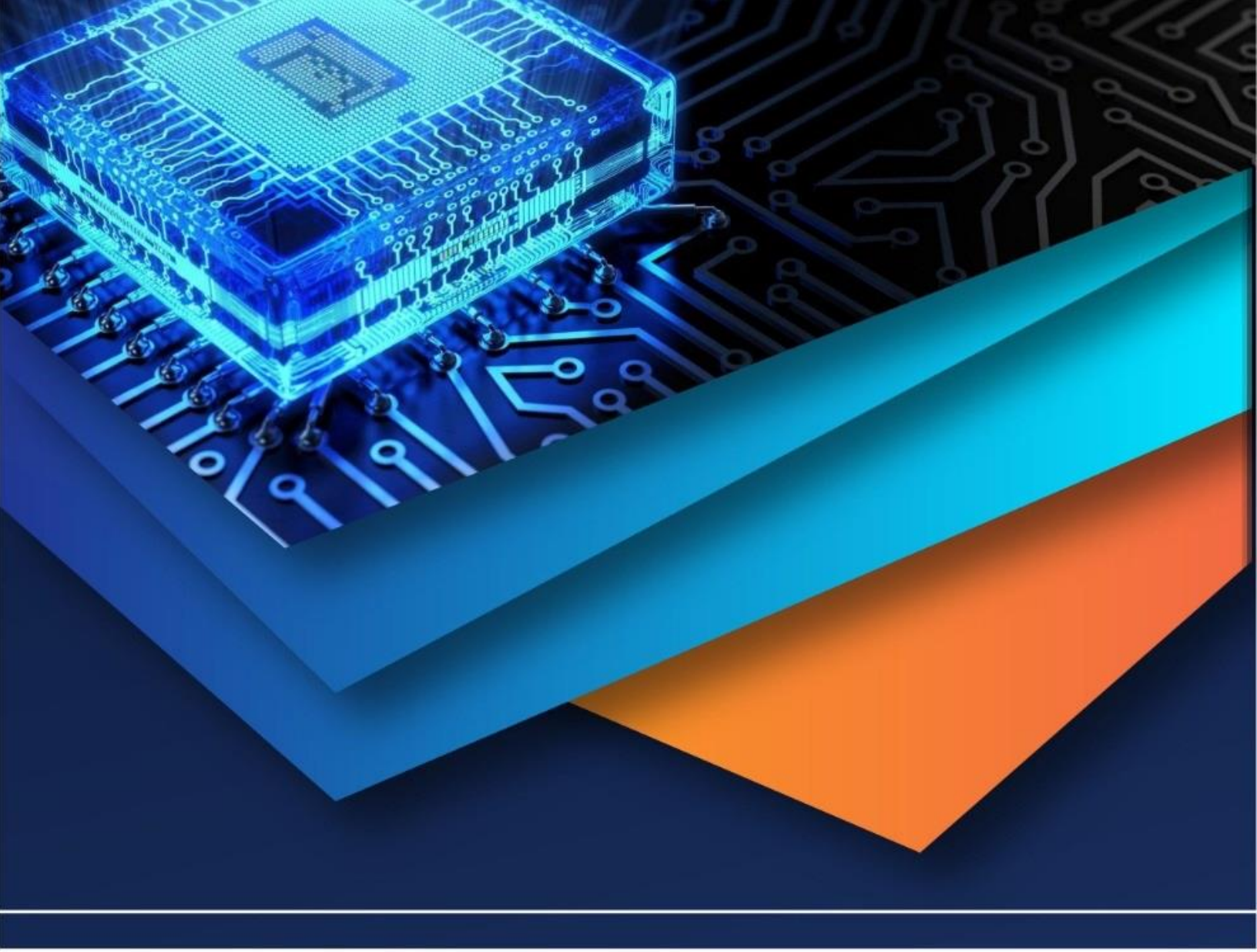

10.22214/IJRASET

45.98

IMPACT FACTOR: 7.129

IMPACT FACTOR: 7.429

INTERNATIONAL JOURNAL FOR RESEARCH

IN APPLIED SCIENCE & ENGINEERING TECHNOLOGY